Detection of Manhole Covers in High-Resolution Aerial Images of Urban Areas by Combining Two Methods

Jérôme Pasquet, Thibault Desert, Olivier Bartoli, Marc Chaumont, Carole Delenne, Gérard Subsol, Mustapha Derras, and Nanée Chahinian

***Abstract*—Mispositioning of buried utilities is an increasingly important problem both in industrialized and developing countries because of urban sprawl and technological advances. However, some of these networks have surface access traps, which may be visible on high-resolution airborne or satellite images and could serve as presence indicators. We put forward a methodology to detect manhole covers and grates on very high-resolution aerial and satellite images. Two methods are tested: the first is based on a geometrical circular filter, whereas the second one uses machine learning to retrieve some patterns. The results are compared and combined to benefit from the two approaches.**

***Index Terms*—Buried utility network, circular object detection, geometrical filter, high resolution, machine learning.**

I. Introduction

REGARDLESS of economic growth, urban expansion is an ongoing trend [1], [2], and urban areas are viewed as particularly vulnerable to climate change; current forecasts predict increasing poverty and rapid urbanization [3]. Hence, urban areas are highly sensitive and need frequent monitoring. One of the direct consequences of urban expansion is the development of underground utility networks. Over the past century, it was a common practice for public service providers to install, operate, and repair their networks separately [4]. Hence, it is now very difficult to find accurate records of utility network maps. Mispositioning of buried utilities is an increasingly important problem both in industrialized and developing countries because of urban sprawl and technological advances that create new needs among consumers resulting in additional cables and pipes that have to be added and connected [5], [6]. Urban works will thus be more prone to delays with concomitant additional costs [7], [8]. Locating past records can be a cumbersome and time-consuming task. An alternative would be to use a quick survey method to have an estimate of the current situation. Some of these buried networks have surface access traps, which may be visible on high-resolution airborne or satellite images. Indeed, high spatial resolution imagery is becoming more and more available. There is a growing number of cities that provide high-resolution (< 20 cm/pixel) orthophotos through open data platforms, i.e., free of charge. If correctly detected, these elements could serve as indicators of underground utility networks. Furthermore, they can be used as landmarks in photogrammetric applications [9] or in geotechnical works such as subsidence calculations [10]. We put forward a methodology to detect small urban objects, namely, manhole covers and grates, on very high-resolution aerial and satellite images. Two methods are tested: the first is based on a geometrical circular filter, whereas the second one uses machine learning to retrieve some patterns. The results are compared and combined to benefit from the two approaches.

Manuscript received June 30, 2015; revised October 27, 2015; accepted November 12, 2015. Date of publication January 05, 2016; date of current version April 22, 2016. This work was supported in part by the Programme National de Télédétection Spatiale (PNTS, http://www.insu.cnrs.fr/actions-sur-projets/pnts-programme-national-deteledetection-spatiale) under Grant PNTS-2014-01, and in part by the public funds received in the framework of GEOSUD, a project (ANR-10-EQPX-20) of the program "Investissements d'Avenir" managed by the French National Research Agency.

J. Pasquet is with Berger-Levrault, 31676 Labège, France, and also with Montpellier Laboratory of Informatics, Robotics, and Microelectronics (LIRMM), University of Montpellier, CNRS, 34090 Montpellier, France (e-mail: pasquet@lirmm.fr).

T. Desert, O. Bartoli, and N. Chahinian are with the Institut de Recherche pour le Dveloppement (IRD), UMR HSM 5569, CNRS, Université de Montpellier, 34090 Montpellier, France.

M. Chaumont is with the University of Nimes, 30000 Nimes, France, and also with Montpellier Laboratory of Informatics, Robotics, and Microelectronics (LIRMM), University of Montpellier, CNRS, 34090 Montpellier, France.

C. Delenne is with UMR HSM 5569, CNRS, Institut de Recherche pour le Dveloppement (IRD), University of Montpellier, 34090 Montpellier, France.

G. Subsol is with Montpellier Laboratory of Informatics, Robotics, and Microelectronics (LIRMM), CNRS, University of Montpellier, 34090 Montpellier, France.

M. Derras is with Berger-Levrault, 31676 Labège, France.

Digital Object Identifier 10.1109/JSTARS.2015.2504401

II. Materials and Methods

The methodology is tested on a small town in southern France (Gigean, Herault).

A. Data

Three images with different resolutions were used to put forward the method. Pléiade bundle products (50-cm resolution) obtained through the SUDOC project and orthophotos (Fig. 1) of the town of Gigean (Herault, South of France) with a 25-cm resolution provided by SIG-LR, and were used in the pretreatment step of the methodology. Supplementary high-resolution orthorectified aerial photographs (5300×5500 pixels at 4-cm resolution) were specifically acquired, since the machine-learning method requires a very high resolution (see Fig. 2). Ground truth was acquired on three residential zones (zones 1–3 in Fig. 1).

The methodology is threefold. First, the image is segmented to extract the zones where manhole covers and grates can be

1939-1404 © 2015 IEEE. Personal use is permitted, but republication/redistribution requires IEEE permission.
See http://www.ieee.org/publications_standards/publications/rights/index.html for more information.

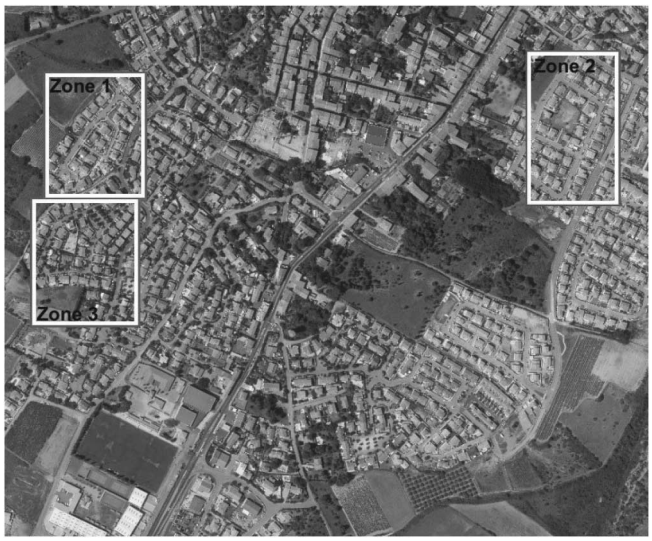

Fig. 1. Orthophoto of Gigean, south of France SIG-LR 2014, and location of the three testing zones used to validate the approach.

Fig. 2. Extract of the 4-cm resolution image.

found, i.e., roads, streets, and pavements. Then, the vegetation and shadows are eliminated by using colorimetric indices, using infrared information provided by the Pléiade images. Finally, either the circular object detection method proposed in [11] or the machine-learning approach is used to locate the manhole covers and grates. These two methods are compared and merged to increase the detection performance.

B. Pretreatment Procedure

1) Roads Detection: Several methods were tested to extract the roads. The most efficient one in terms of implementation simplicity, calculation time, and final results consists in selecting all the light-gray pixels in the image, i.e., pixels having a low intensity in all channels of the image. The average value of each pixel over the three channels (red, green, and blue) is computed, and the pixel is classified as "road," if its radiometric value in each channel deviates from the mean value by less than a given threshold. In this application, the threshold was set

Fig. 3. Roads detection using gray-level threshold and extraction of the biggest connected components.

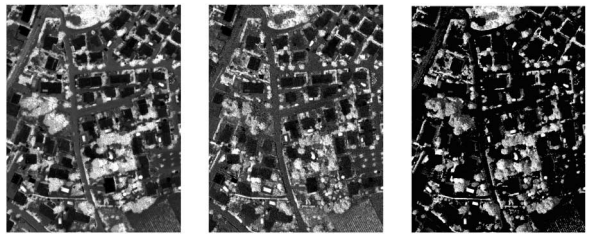

Fig. 4. Detection of vegetation using left: NDVI; middle: ExG; and right: fusion of the two previous results. White pixels belong to the vegetation class.

to 10%. Classified pixels are then merged into connected components using the union-find algorithm. The roads are expected to constitute large connected components; hence, the smallest units (smaller than 1000 pixels) are eliminated. Fig. 3 shows the orthophoto after the road-detection step.

2) Vegetation and Shadow Removal: Two indices are used to segment the vegetation. The classical NDVI uses the near-infrared (NIR) information of the Pléiades images in contrast to the red (R) band

$$\mathrm{NDVI} = \frac{\mathrm{NIR} - \mathrm{R}}{\mathrm{NIR} + \mathrm{R}}. \tag{1}$$

The ExG index (Excess Green) is used on the areal orthophotos, which do not have a NIR channel; it is defined as

$$\mathrm{ExG} = 2\mathrm{G} - \mathrm{R} - \mathrm{B} \tag{2}$$

The results are then combined to benefit from the spectral resolution of the Pléiades images and the spatial resolution of the orthophotos (see Fig. 4).

The shadow elimination procedure is based on Dempster-Shafer's evidence theory following a method presented in [12]. A final smoothing using the iterated conditional modes (ICM) algorithm [13] is performed (Fig. 5). The resulting shadow characteristic image is then combined with the vegetation image to clean the orthophotos from areas not supposed to contain manhole covers.

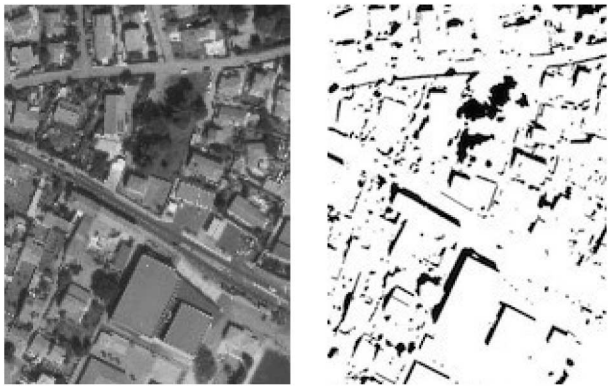

Fig. 5. Shadow elimination from [12] and smoothing using an ICM algorithm.

C. Circular Object Detection

The geometrical approach is based on the method proposed in [11] for the detection of circular patterns in a noisy and low-contrasted image. The authors put forward a filter that consists of two annular regions R_1 and R_2 of radius r_1 to r and r to r_2, each of which is divided into eight subregions (see Fig. 6). The filter is applied to a gray-scaled image, obtained with the luminance formula.

Three indices are computed to detect a circular pattern on a sliding window, using normalized histograms of each region/subregion. The first one estimates the similarity between two statistical distributions using the Bhattacharyya coefficient

$$\mathrm{S}(R_1, R_2) = \sum_{l=1}^{L} \sqrt{p_1(l) p_2(l)} \tag{3}$$

where p_1 (respectively p_2) is the normalized histogram of R_1 (respectively R_2) and L is the maximal intensity of the two histograms. The result of this index is 1.0 when the two histograms are identical and 0.0 when they are completely different. The desirable value for this index to isolate a circular pattern from its background is thus lower.

The second index is computed to avoid detection of linear patterns. It is based on the comparison between the intensity distribution of R_1 and those of the eight subregions of R_2

$$\mathrm{S}_8 = \max_{j \in 1,\ldots,8} \left\{ \mathrm{S}(R_1, S_2^j) \right\} \tag{4}$$

where S_2^j denotes the jth subregion of R_2. This index is low when all oriented similarity scores between R_1 and each subregion of R_2 are small.

The last index assesses the uniformity within the two main regions

$$\mathrm{U}(R_i) = \min_{j,j' \in \{1..8\}} \left\{ \mathrm{S}(S_i^j, S_i^{j'}) \right\} \tag{5}$$

where i stands for the region and j, j' for the subregions. The three indices are finally merged into a global index for circular pattern detection

$$\zeta = (1 - \max\{\mathrm{S}(R_1, R_2), \mathrm{S}_8\}) \cdot \mathrm{U}(R_1) \cdot \mathrm{U}(R_2). \tag{6}$$

The higher the value of ζ, the higher the probability of encountering a circular shaped object.

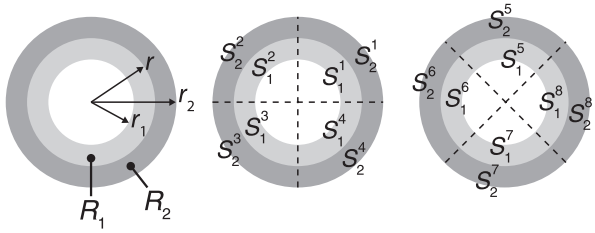

Fig. 6. Circular filter (from [11]). Left: R_1 and R_2 are the two main regions; middle and right: definition of the subregions (the phase shift is $\pi/4$).

TABLE I
DETECTION RESULTS IN RESIDENTIAL AREAS

Zones	1	2	3
Manholes per zone (nb)	26	19	19
Detected objects (nb)	23	21	13
True positives (nb)	12	11	4
False positives (nb)	11	10	9
Detected manholes (%)	46%	58%	21%
Undetected manholes (%)	54%	42%	79%
False detection (%)	47%	47%	69%

Fig. 7. Examples of results. Left: true positive; middle: undetected; right: false positive.

D. Machine-Learning Approach

The circular object detection is only efficient when there is an average color difference between the inside and outside circles. Moreover, this approach does not use the texture information inside the circle to decide on the manhole cover identification. To overcome these problems, we use a machine-learning algorithm which builds the best model from the data. This method is quite efficient for urban object detection [14]. The learning phase involves three steps [15].

1) Extraction of a sample composed of manhole covers and small random images from the training database (each extract being resized to a constant size for the sake of robustness at all scales).
2) Extraction of multiple histograms from oriented gradients (HOG) [16] to transform data into feature vectors measuring the distribution of the gradient angles within the image.
3) Application of a linear SVM classifier [17] to create the required model.

The scene covered by the 4-cm image contained 125 manholes, with an average size of 80×80 cm, 91 of which were used to build the training set and 34 for the testing step. During the evaluation step, a multiscale representation of the testing image called "pyramid" is used. The pyramid approach allows us to find manhole covers with different sizes. A sliding window is applied on each pyramid to localize the manhole cover.

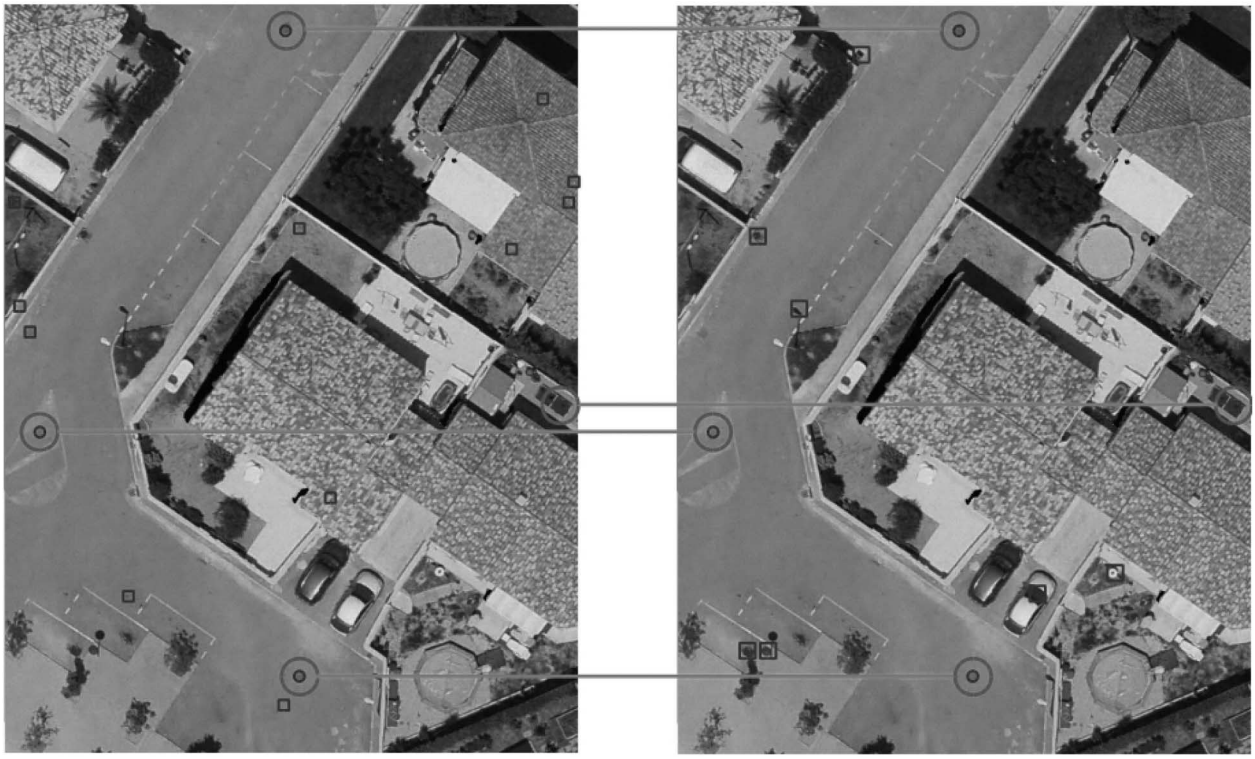

Fig. 8. Two figures represent the results obtained with the circular filter on the left and the machine-learning method on the right. The rectangles are the true negatives and the circles are the true positives. The lines connect the two common results between two approaches. The testing image is at 4-cm resolution.

During the process, the training classifier gives a score for recognized manhole covers at each position.

E. Merging the Approaches

The significant difference between the two approaches stems from the fact that the first one uses pixel intensity to detect a circular shape while the second one is based on a model of the object, built from the gradient. We observed that the detection errors differ from one approach to the other. Therefore, we combined the results from the two methods to increase the detection performance. The final score is obtained by merging the scores given by each approach. Let $f(x)$ be a function that returns the value of ζ for a pixel x (6) rescaled between 0 and 100, and $g(x)$ is a function that returns the probability of a pixel x being a manhole cover center by the machine-learning approach. The product function between f and g is called h (7) and is used as a score value for the presence of manhole covers. Note that all the objects may not be detected by both methods. For instance, function f returns a null score for rectangular shapes. We thus suggest other functions for scoring the presence of a manhole cover $s(x)$ for the sum (8), $n(x)$ and $m(x)$ for the min and max (9) and (10). Scoring functions are evaluated in Section III.

$$h(x) = f(x) \cdot g(x) \tag{7}$$

$$s(x) = \begin{cases} 2.f(x), & g(x) = 0 \\ 2.f(x), & f(x) = 0 \\ (x) + g(x), & \text{otherwise} \end{cases} \tag{8}$$

$$n(x) = \min(f(x), g(x)) \tag{9}$$

$$m(x) = \max(f(x), g(x)). \tag{10}$$

III. Results

The circular method was first applied on three test zones extracted from the orthophoto image, corresponding to housing estates for which the ground truth is available.

The primary results indicate (Table I) that the filter is able to detect manhole covers, in all three zones with slightly better results for zone 2 and poorer results for zone 3. As the three zones are residential areas with similar semi-detached houses, the difference in results is thought to be caused by a higher proportion of vegetation and shadows. Fig. 7 shows examples of true and false positives as well as undetected objects.

The results also highlight the existence of false positives, reaching nearly 60% in zone 3. No clear typology of the situations which lead to false detection can be made at this stage. Over the three zones, 42%–79% of manholes remain undetected. This may seem as a poor result; however, it is a common practice in southern France not to systematically take down all manhole locations during surveying, but rather to register only half or one-third of covers each time, in an effort to cut down costs.

The two methods have then been applied on the 4-cm resolution image (see Fig. 8). Their results are compared in terms of precision and recall

$$\text{precision} = \frac{\text{TP}}{\text{TP} + \text{FP}} \quad \text{recall} = \frac{\text{TP}}{\text{TP} + \text{FN}} \tag{11}$$

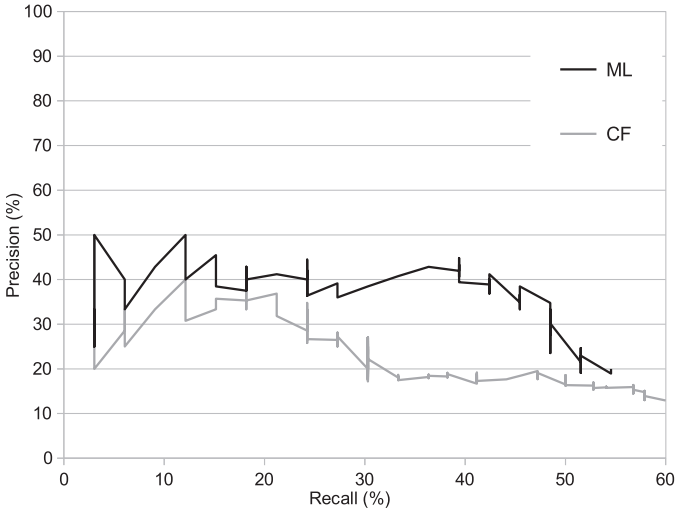

Fig. 9. Precision versus recall, with circular pattern detection (CF) and machine-learning method (ML).

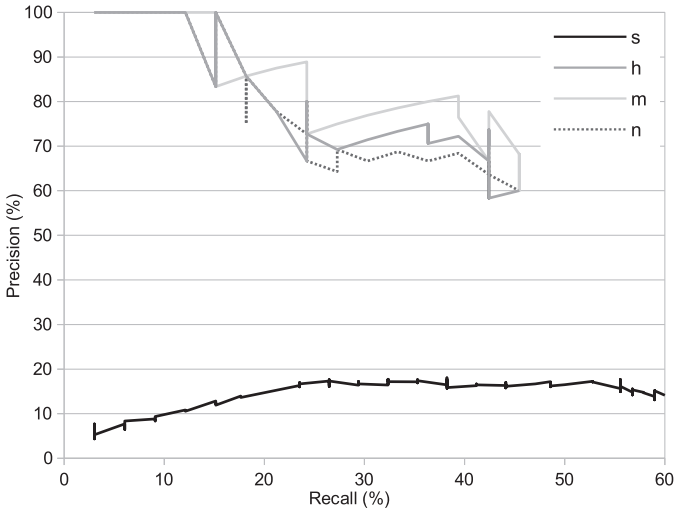

Fig. 10. Results of the combined method: sum (s), product (h), maximum (m), and minimum (n) functions. Comparison with the two approaches (ML: machine learning) and (CF: circular filter).

where TP stands for *true positive*, number of correctly detected manhole covers; FN for *false negative*, number of omitted manhole covers; and FP for *false positive*, number of objects confused as manhole covers. TP + FP is thus the total number of detected objects.

Fig. 9 shows the performance of the circular-detection filter method using a receiver operating characteristics (ROC) graph [18], i.e., precision as a function of the recall, where the threshold applied to ζ varies. All manhole covers could not be detected by this method, because about 20% of them had a rectangular shape and were undetectable. We also noticed a significant number of false positives. In fact, there were many circular patterns on the road such as oil spots or potholes, which are enhanced as the image is smoothed.

The ROC curve of the machine-learning method, which has higher precision than the previous one, is also plotted in Fig. 9. Poor results are obtained: for a recall of 50%, only 20% of the objects were manhole covers. They may stem from the small size of the training database.

Fig. 10 shows the combined method, with functions h, s, n, and m. All these functions but s give better results than the two methods taken separately. The poorer results obtained with the summing function s were due to the addition of all detections, including false ones. Hence, the precision was worsened according to (11).

With for the other functions (m, n, and h), the precision was increased by more than 25%. For instance, a recall of 40% corresponded to a precision of approximately 43% for the machine-learning approach (ML curve) and reached 68% for the min function (n curve).

We noticed that the maximum function m gave a better score: nearly twice the precision of the machine-learning method. Actually, if the classifier probability value is high, then this response is more efficient than the dot or minimum return. This could have two explanations. First, nearly ideal circular shapes may be detected with high precision by the circular filter, but may have a lower probability with the machine-learning method, which has no information on the shape. In contrast, the circular filter gives a lower score for rectangular manhole covers, contrary to the machine-learning approach, which is more robust.

The main shortcomings of this kind of approach are that, when using two methods, the combined recall value is always lower than the lowest score of each method taken separately.

IV. Conclusion

The objective of this work was to put forward a methodology to detect small urban objects on high-resolution images to reconstruct buried utility networks. The main challenge was to detect gray objects, whose size is within the spatial resolution limit of the image, that are located on a gray background.

The preliminary results obtained using the geometrical filter are satisfactory, as they allow the detection of 42% of manhole covers in residential areas. Surveying companies in southern France are often required to report one-third of manholes to cut down production costs. Our method thus allows the same detection rate. However, the rate of false negatives is still unacceptably high and remains unchanged even when using higher resolution images (4-cm resolution). Additional criteria can be used to discriminate these false negatives, such as the density of detected objects. Furthermore, we are currently investigating the use of alternative remote-sensing data such as thermal or infrared images, to improve the detection rate.

Regarding the machine-learning method, the results show that nearly 40% of manhole covers were detected with a precision of 80%. These results are encouraging, specially considering that a small training database was used.

Many options remain unexplored and will be investigated in the very near future. For instance, a square filter could be added to the geometrical detection procedure, additional SVMs could be tested as well as other combined methods [19]. The high resolution of the aerial images for the localization of small urban objects is a highly promising research field.

The final objective of this project is to estimate urban contribution to downstream waterbodies and not to precisely assess water fluxes in the buried network itself. Based on the detected manhole covers locations, and knowing the efficiency of the method, a network will be statistically reconstructed using the rules and regulations of drainage network implementation in France.

A sensitivity analysis will also be performed to estimate the impact the partial information on network characteristics have on the assessment of downstream fluxes.

ACKNOWLEDGMENT

The orthophotos of Gigean were kindly provided by SIG-LR.

REFERENCES

[1] S. Poelhekke, "Urban growth and uninsured rural risk: Booming towns in bust times," *J. Dev. Econ.*, vol. 96, pp. 461–475, 2011.
[2] D. Burns, V. T. J. McDonnell, J. Hasseth, J. Duncan, and C. Kendall, "Effects of suburban development on runoff generation in the croton river basin, new york, USA," *J. Hydrol.*, vol. 311, pp. 266–281, 2005.
[3] R. Gasper, A. Blohm, and M. Ruth, "Social and economic impacts of climate change on the urban environment," *Curr. Opin. Environ. Sustain.*, vol. 3, pp. 150–157, 2011.
[4] C. Rogers *et al.*, "Condition assessment of the buried utility service infrastructure: A proposal for integration." *Tunnell. Underground Space Technol.*, vol. 28, pp. 202–211, 2012.
[5] H. Jamil, N. Z., and M. Mohid Yussof, "Underground utility mapping and its challenges in malaysia," in *Proc. FIG Working Week. Know. Manage Territory Protect Environ. Evaluate Cult. Heritage*, Rome, Italy, 2012, p. 15.
[6] N. Metje *et al.*, "Mapping the underworld: State of the art review," *Tunnell. Underground Space Technol.*, vol. 22, pp. 568–586, 2007.
[7] Y. Yung, "Evaluation of subsurface utility engineering for highway projects: Benefit-cost analysis," *Tunnell. Underground Space Technol.*, vol. 27, pp. 111–122, 2012.
[8] H. Jeong, D. Abraham, and J. Lew, "Evaluation of an emerging market in subsurface utility engineering," *J. Constr. Eng. Manage.*, vol. 130, no. 2, pp. 225–234, 2004.
[9] C. Drewniok and K. Rohr, "Exterior orientation-an automatic approach based on fitting analytic landmark models," *ISPRS J. Photogramm. Remote Sens.*, vol. 52, pp. 132–145, 1997.
[10] G. Liu, H. Jia, R. Zhang, H. Zhang, H. Lia, and M. Sang, "Exploration of subsidence estimation by persistent scatterer insar on time series of high resolution terrasar-x images," *IEEE J. Sel. Topics Appl. Earth Observ. Remote Sens.*, vol. 4, no. 1, pp. 159–170, Mar. 2011.
[11] H. Niigaki, J. Shimamura, and M. Morimoto, "Circular objet detection based on seperability and uniformity of feature distributions using bhattacharrya coefficient," in *Proc. 21st Int. Conf. Pattern Regocnit. (ICPR'12)*, Tsukuba, Japan, 2012, pp. 2009–2012.
[12] T. T. Ngo, Ch. Collet, and V. Mazet, "Détection simultanée de l'ombre et la végétation sur des images aériennes couleur en haute résolution," *Traitement du signal, special issue*, vol. 32, no. 2–3, pp. 311–333, 2015.
[13] R. Glendinning, "An evaluation of the ICM algorithm for image reconstruction," *J. Stat. Comput. Simul.*, vol. 3, no. 31, pp. 169–185, 1989.
[14] M. Chaumont, L. Tribouillard, G. Subsol, F. Courtade, J. Pasquet, and M. Derras, "Automatic localization of tombs in aerial imagery: Application to the digital archiving of cemetery heritage," in *Proc. Digit. Heritage Int. Congr.*, vol. 1, 2013, pp. 657–660.
[15] P. Viola and M. Jones, "Rapid object detection using a boosted cascade of simple features," in *Proc. Comput. Vis. Pattern Recognit.*, 2001, pp. 511–518.
[16] Q. Qiang, S. Avidan, M. Yeh, and K. Cheng, "Fast human detection using a cascade of histograms of oriented gradients," in *Proc. Comput. Vis. Pattern Recognit.*, pp. 1491–1498, 2006.
[17] R. Fan, K. Chang, C. Hsieh, and C. Lin, "LIBLINEAR: A library for large linear classification," *J. Mach. Learn. Res.*, vol. 9, pp. 1871–1874, 2008.
[18] T. Fawcett, "An introduction to ROC analysis," *Pattern Recognit. Lett.*, vol. 27, pp. 861–874, 2006.
[19] J. Kittler, M. Hatef, R. P. W. Duin, and J. Matas, "On combining classifiers," *IEEE Trans. Pattern Anal. Mach. Intell.*, vol. 20, no. 3, pp. 226–239, Mar. 1998.

Jérôme Pasquet received the Master's degree in computer science from the University of Montpellier II, Montpellier, France, in 2013 and is currently pursuing the Ph.D. degree at LIRMM (Montpellier Laboratory of Informatics, Robotics and Microelectronics), Montpellier, France.

His research interests include urban objects detection and segmentation in aerial photography.

Thibault Desert received the M.Sc. degree in applied mathematics from the French National Institute of Applied Sciences (INSA), Toulouse, France, in 2015 and is currently pursuing the Ph.D. degree in aerodynamic design at ONERA, Châtillon, France.

He worked as a Research Fellow in the project PNTS 2014-1.

Olivier Bartoli received the M.Sc. degree in image treatment from the University of Montpellier, Montpellier, France, in 2014. He did a six-month internship at UMR HydroScience Montpellier, Montpellier, France.

He worked as a Research Fellow in the projet PNTS 2014-1. He is currently working as a Consultant for a global asset-servicing provider.

Marc Chaumont received the Engineer Diploma degree in computer science from the INSA, Rennes, France, in 1999, the Ph.D. degree from the IRISA, Rennes, France, in 2003, and the HDR "Habilitation à Diriger des Recherches" from the University of Montpellier, Montpellier, France, in 2013.

Since September 2005, he has been working as an Assistant Professor with the LIRMM laboratory of Montpellier and the University of Nmes, Nimes, France. His research interests include multimedia security (steganography, watermarking, digital forensics, video and image compression) and segmentation and tracking in images and videos.

Dr. Chaumont is a member of the TC of IEEE SPS—Information Forensics and Security for the period 2015–2017. He was a Program Chair of ACM IH&MMSec'2013. He is a Reviewer for more than 20 journals (IEEE TIFS, IS&T JEI, etc.) and for more than 10 conferences (EI MWSF, IEEE WIFS, ACM IH&MMSec, IEEE ICIP, etc.).

Carole Delenne received the M.Sc. degree in applied mathematics from the University of Toulouse, Toulouse, France, in 2003, and the Ph.D. degree in remote sensing from the University of Montpellier, Montpellier, France, in 2006.

Since 2007, she has been working as a Lecturer with the University of Montpellier. Her research interests include hydraulic modeling, sensitivity analysis, and remote sensing for the calibration and validation of hydrodynamics models.

Gérard Subsol received the Ph.D. degree in computer science from the INRIA Sophia Antipolis, Valbonne, France in 1995.

He was the Expert-Engineer with INRIA Sophia Antipolis, Research Engineer with University of Avignon, Avignon, France, and R&D Engineer with the start-up company Intrasense, Montpellier, France. Since 2006, he has been working as a CNRS Researcher with LIRMM, Montpellier, France. He is currently working on several applications of 2-D and 3-D image processing.

Mustapha Derras received the Ph.D. degree in computer science from the LASMEA, Clermont-Ferrand, France, in 1993.

He is currently the Director of Technology, Innovation, and Research, Berger-Levrault, Labége, France. Previously, he held positions with the aim of creating innovative new products as Business Unit Director Catia, Dassault Systmes, Marketing, and R&D at TIMEG, Director of Business Unit CAT at Cadence Design Systems, Software Development Architect at General Electric Medical Systems, and Project Manager at CLAAS, where he completed his mobile robotics and image processing studies.

Nanée Chahinian received the Ph.D. degree in water sciences from the University of Montpellier, Montpellier, France.

He is a Researcher with the Institut de Recherche pour le Dveloppement (IRD). From 2009 to 2012, she worked in Morocco on an EU funded research project and was confronted with the lack of data regarding underground water networks. Her research interests include urban hydrology and rainfall-runoff modelling.